Available online at www.sciencedirect.com
SCIENCE DIRECT
Journal of Computational Physics 216 (2006) 403–429
JOURNAL OF COMPUTATIONAL PHYSICS
www.elsevier.com/locate/jcp

MUSTA fluxes for systems of conservation laws

E.F. Toro *, V.A. Titarev

Laboratory of Applied Mathematics, Faculty of Engineering, University of Trento, Mesiano, 38050, Trento, Italy

Received 16 December 2004; received in revised form 13 September 2005; accepted 14 December 2005
Available online 24 February 2006

Abstract

This paper is about numerical fluxes for hyperbolic systems and we first present a numerical flux, called GFORCE, that is a weighted average of the Lax-Friedrichs and Lax-Wendroff fluxes. For the linear advection equation with constant coefficient, the new flux reduces identically to that of the Godunov first-order upwind method. Then we incorporate GFORCE in the framework of the MUSTA approach [E.F. Toro, Multi-Stage Predictor–Corrector Fluxes for Hyperbolic Equations. Technical Report NI03037-NPA, Isaac Newton Institute for Mathematical Sciences, University of Cambridge, UK, 17th June, 2003], resulting in a version that we call GMUSTA. For non-linear systems this gives results that are comparable to those of the Godunov method in conjunction with the exact Riemann solver or complete approximate Riemann solvers, noting however that in our approach, the solution of the Riemann problem in the conventional sense is avoided. Both the GFORCE and GMUSTA fluxes are extended to multi-dimensional non-linear systems in a straightforward unsplit manner, resulting in linearly stable schemes that have the same stability regions as the straightforward multi-dimensional extension of Godunov's method. The methods are applicable to general meshes. The schemes of this paper share with the family of centred methods the common properties of being simple and applicable to a large class of hyperbolic systems, but the schemes of this paper are distinctly more accurate. Finally, we proceed to the practical implementation of our numerical fluxes in the framework of high-order finite volume WENO methods for multi-dimensional non-linear hyperbolic systems. Numerical results are presented for the Euler equations and for the equations of magnetohydrodynamics.

Keywords: Hyperbolic conservation laws; Upwind methods; GFORCE flux; MUSTA fluxes; WENO methods; Euler equations; MHD equations

1. Introduction

Numerical methods for solving non-linear systems of hyperbolic conservation laws via finite volume methods or discontinuous Galerkin finite element methods require, as the building block, a monotone numerical flux. The choice of the building block has a profound influence on the properties of the resulting schemes. There are essentially two approaches for providing a monotone numerical flux, the simplest of

* Corresponding author. Tel.: +39 0461 882674; fax: +39 0461 882676.
E-mail addresses: toro@ing.unitn.it (E.F. Toro), titarev@ing.unitn.it (V.A. Titarev).
URLs: http://www.ing.unitn.it/toro (E.F. Toro), http://www.science.unitn.it/titarev (V.A. Titarev).

0021-9991/$ - see front matter
doi:10.1016/j.jcp.2005.12.012

which utilizes a symmetric stencil and does not explicitly make use of wave propagation information, giving rise to *centred* or *symmetric* schemes [19,13,15,18,38,41,21,4]. A more refined approach utilizes wave propagation information contained in the differential equations. This is done through the exact or approximate solution of the Riemann problem, giving rise to *upwind* methods [7,12,26,46,28]. For up-to-date background on these methods see, for example [11,39,20,17].

Within the class of existing monotone first-order fluxes, the first-order upwind scheme of Godunov is the best, it has the smallest local truncation error. However, the superior accuracy of established upwind methods comes at a cost, one must solve exactly or approximately, the Riemann problem. Conventional Riemann solvers are usually complex and for many hyperbolic systems of practical interest are not available, such as for models for compressible multi-phase flows. It is thus desirable to construct a numerical flux that emulates the best flux available (upwind) with the simplicity and generality of symmetric schemes.

In this paper we first present a new flux, called GFORCE, that is a particular average of symmetric fluxes and which reproduces Godunov's upwind scheme for the linear advection equation with constant coefficient. For non-linear systems, it is found that this flux gives superior results to those of the whole family of *incomplete* Riemann solvers that do not explicitly account for linearly degenerate fields, such as the HLL Riemann solver [14] and flux vector splitting schemes. Then we build upon the newly proposed MUSTA (multi-staging) approach [34] to construct schemes that have the simplicity and generality of symmetric schemes and accuracy that is comparable to that of the best upwind schemes for general hyperbolic systems. This is achieved by incorporating the GFORCE flux into the MUSTA approach, as predictor and corrector. It is found that for the linear advection equation with constant coefficient the resulting MUSTA schemes reproduce the Godunov upwind scheme identically, for any number of stages. For non-linear systems, the MUSTA scheme with one or two stages gives results that are indistinguishable from those of *complete* Riemann solvers, such as the exact Riemann solver, Roe's approximate Riemann solver [28] and HLLC [45,42].

For multi-dimensional hyperbolic systems, we utilize the proposed numerical fluxes in the setting of straightforward unsplit finite volume schemes, in which the numerical fluxes are evaluated along the direction normal to the interface, at each integration point. For the linear advection equation with constant coefficients, the resulting *simultaneous updating* schemes are linearly stable in two and three space dimensions and the stability region is identical to that of the Godunov upwind method. The proposed numerical fluxes are used in the setting of TVD schemes and in the framework of WENO finite volume methods for one and multi-dimensional non-linear hyperbolic systems. Finally, we assess the performance of the schemes on carefully chosen test problems and show results for the one- and two-dimensional Euler equations and for the equations of Magnetohydrodynamics in one space dimension.

The rest of the paper is organized as follows: Section 2 introduces the finite volume framework and recalls well-known numerical fluxes. In Section 3 we present the new numerical flux GFORCE. In Section 4 we incorporate this flux into the MUSTA framework. In Section 5 we illustrate the application of the proposed schemes to the solution of various hyperbolic problems. Conclusions are drawn in Section 6. In the Appendix we give an algorithm in the form of a FORTRAN program to compute an example of a numerical flux, as proposed in this paper.

2. The framework

Finite volume and discontinuous Galerkin finite element methods rely on a monotone, first-order intercell numerical flux, the building block of the schemes. Here, we are concerned with numerical fluxes in the frame of the finite volume approach.

2.1. Finite volume schemes

For the purpose of this section it is sufficient to consider a time-dependent non-linear system of hyperbolic conservation laws in two space dimensions

$$\partial_t \mathbf{Q} + \partial_x \mathbf{F}(\mathbf{Q}) + \partial_y \mathbf{G}(\mathbf{Q}) = 0, \tag{1}$$

in which $\mathbf{Q}$ is the vector of conserved variables and $\mathbf{F}(\mathbf{Q})$ and $\mathbf{G}(\mathbf{Q})$ are the vectors of fluxes in the Cartesian coordinate directions x and y, respectively. In the presence of discontinuous solutions one uses the integral form of (1), which is obtained, for example, by integrating (1) on a control volume V with boundary A, leading to

$$\frac{\mathrm{d}}{\mathrm{d}t}\int\int_V \mathbf{Q}\,\mathrm{d}V = -\int_A (\mathbf{F},\mathbf{G})\cdot\mathbf{n}\,\mathrm{d}A. \tag{2}$$

Here $\mathbf{n}$ is the unit vector normal to the boundary A pointing in the outward direction. In the finite volume approach one does not require a change of coordinates, such as body-fitted coordinates, to deal with domains whose boundaries are not aligned with the Cartesian directions. Discretization can be performed directly in physical space. Assuming the domain of interest has been discretized by an appropriate mesh, we then apply (2) to a finite volume, or cell, V_i to construct numerical schemes. In particular, a fully discrete finite volume scheme reads

$$\mathbf{Q}_i^{n+1} = \mathbf{Q}_i^n - \frac{\Delta t}{\Delta V_i}\sum_{s=1}^{N} L_s \mathbf{T}_s^{-1}\mathbf{F}_{(i,s)}. \tag{3}$$

Here $\mathbf{Q}_i^n$ is the integral average of $\mathbf{Q}$ in volume V_i at time level n, ΔV_i is the area of V_i, Δt is the time step, N is the total number of faces of V_i, L_s is the length of face s, $\mathbf{T}_s$ is the rotation matrix corresponding to side s and $\mathbf{T}_s^{-1}$ is its inverse, $\mathbf{F}_{(i,s)}$ is the numerical flux for face s in the direction u normal to it, and is obtained by solving the Riemann problem in the direction u, namely:

$$\left.\begin{aligned} &\partial_r \mathbf{Q} + \partial_u \mathbf{F}(\mathbf{Q}) = 0, \quad u \in (-\infty,\infty), \quad r > 0 \\ &\mathbf{Q}(u,0) = \begin{cases} \mathbf{Q}_i^0 = \mathbf{T}_s(\mathbf{Q}_i^n) & \text{if } u < 0, \\ \mathbf{Q}_s^0 = \mathbf{T}_s(\mathbf{Q}_s^n) & \text{if } u > 0. \end{cases} \end{aligned}\right\} \tag{4}$$

Here $r = t - t^n$ is local time; $\mathbf{Q}_s^n$ is the integral average of the conserved variable vector in the control volume adjacent to V_i having s as a common face. T_s aligns the original initial data in the normal direction u to the interface s, prior to solving the Riemann problem. The inverse matrix T_s^{-1} restores back the flux information to the Cartesian frame.

From this point on, the discussion on the numerical flux in an arbitrary direction u can be reduced to that of the *augmented* one-dimensional problem in the x-direction, say, without loss of generality.

2.2. Numerical fluxes

Consider the $m \times m$ one-dimensional system of hyperbolic conservation laws

$$\partial_t \mathbf{Q} + \partial_x \mathbf{F}(\mathbf{Q}) = \mathbf{0}, \tag{5}$$

where $\mathbf{Q}$ is a vector of m components, the conserved variables, and $\mathbf{F}(\mathbf{Q})$ is the corresponding vector of fluxes. The finite volume scheme to solve (5) reads

$$\mathbf{Q}_i^{n+1} = \mathbf{Q}_i^n - \frac{\Delta t}{\Delta x}[\mathbf{F}_{i+\frac{1}{2}} - \mathbf{F}_{i-\frac{1}{2}}], \tag{6}$$

where $\mathbf{F}_{i+\frac{1}{2}}$ is the numerical flux, Δx is the length of the control volume and Δt is the time step.

Godunov's upwind method [12] defines the intercell numerical flux $\mathbf{F}_{i+\frac{1}{2}}$ in terms of the solution, if available, of the corresponding Riemann problem

$$\left.\begin{aligned} &\partial_t \mathbf{Q} + \partial_x \mathbf{F}(\mathbf{Q}) = \mathbf{0}, \quad x \in (-\infty,\infty), \quad t > 0, \\ &\mathbf{Q}(x,0) = \begin{cases} \mathbf{Q}_i^n & \text{if } x < 0, \\ \mathbf{Q}_{i+1}^n & \text{if } x > 0. \end{cases} \end{aligned}\right\} \tag{7}$$

The so-called *Riemann fan* in the $x-t$ plane consists of $m+1$ constant states separated by m wave families, each one associated with a real eigenvalue $\lambda^{(k)}$. The similarity solution of (7) depends on the ratio x/t and is denoted by $\mathbf{Q}_{i+\frac{1}{2}(x/t)}$. The Godunov intercell numerical flux is found by first evaluating $\mathbf{Q}_{i+\frac{1}{2}}(x/t)$ at $x/t=0$, that is along the t-axis, and then evaluating the physical flux vector $\mathbf{F}(\mathbf{Q})$ in (7) at $\mathbf{Q}_{i+\frac{1}{2}}(0)$, namely

$$\mathbf{F}^{\mathrm{GodU}}_{i+\frac{1}{2}} = \mathbf{F}(\mathbf{Q}_{i+\frac{1}{2}}(0)). \tag{8}$$

The exact solution of (7) for complicated systems will generally involve the iterative solution of a non-linear system and thus in practice, whenever available, one uses approximate Riemann solvers. For a review on Riemann solvers see, for example [39].

Non-upwind (or centred, or symmetric) schemes do not explicitly utilize wave propagation information and are thus simpler and more generally applicable. Commonly, the numerical fluxes can be computed explicitly as algebraic functions of the initial condition in (7), namely

$$\mathbf{F}_{i+\frac{1}{2}} = \mathbf{F}_{i+\frac{1}{2}}(\mathbf{Q}^n_i, \mathbf{Q}^n_{i+1}). \tag{9}$$

One may interpret centred fluxes as resulting from a *low-level approximation* to the solution of the Riemann problem (7), in which the Riemann fan *is not opened*. Two classical centred fluxes are the Lax-Friedrichs flux

$$\mathbf{F}^{\mathrm{LF}}_{i+\frac{1}{2}} = \frac{1}{2}[\mathbf{F}(\mathbf{Q}^n_i) + \mathbf{F}(\mathbf{Q}^n_{i+1})] - \frac{1}{2}\frac{\Delta x}{\Delta t}[\mathbf{Q}^n_{i+1} - \mathbf{Q}^n_i] \tag{10}$$

and the two-step Lax-Wendroff flux

$$\mathbf{F}^{\mathrm{LW}}_{i+\frac{1}{2}} = \mathbf{F}(\mathbf{Q}^{\mathrm{LW}}_{i+\frac{1}{2}}), \quad \mathbf{Q}^{\mathrm{LW}}_{i+\frac{1}{2}} = \frac{1}{2}[\mathbf{Q}^n_i + \mathbf{Q}^n_{i+1}] - \frac{1}{2}\frac{\Delta t}{\Delta x}[\mathbf{F}(\mathbf{Q}^n_{i+1}) - \mathbf{F}(\mathbf{Q}^n_i)]. \tag{11}$$

Another, more recent, centred flux is the FORCE flux, which was derived [38] from a deterministic interpretation of the staggered-grid version of Glimm's method [10] and results in a non-staggered one-step conservative scheme of the form (6) with intercell numerical flux

$$\mathbf{F}^{\mathrm{force}}_{i+\frac{1}{2}} = \frac{1}{4}\left[\mathbf{F}(\mathbf{Q}^n_i) + 2\mathbf{F}(\mathbf{Q}^{\mathrm{LW}}_{i+\frac{1}{2}}) + \mathbf{F}(\mathbf{Q}^n_{i+1}) - \frac{\Delta x}{\Delta t}(\mathbf{Q}^n_{i+1} - \mathbf{Q}^n_i)\right] \tag{12}$$

with $\mathbf{Q}^{\mathrm{LW}}_{i+\frac{1}{2}}$ as in (11). For further details on the FORCE flux see [39,41]. See also [4], where convergence is proved for the case of two non-linear hyperbolic systems, namely the equations of isentropic gas dynamics and the shallow water equations with a bottom slope source term.

Note that the FORCE flux (12) is the arithmetic average of the Lax-Friedrichs flux (10) and the two-step Lax-Wendroff flux (11). It is worth noting that there is an analogy between the FORCE scheme [38] and the composite schemes of Liska and Wendroff [22]. The composite schemes advance the solution a given number of time steps by the Lax-Friedrichs method and another number of time steps by the Lax-Wendroff method. In the FORCE scheme the *composite aspect* is found at the level of the flux, which is precisely the arithmetic mean, weight of 1/2, of the Lax-Friedrichs and the Lax-Wendroff fluxes. The weight 1/2 is significant, as it is precisely the value that gives a monotone scheme with the maximum region of monotonicity, without resorting to wave propagation information, as seen in Fig. 1 discussed in the following section.

3. The generalized FORCE flux

Here, we construct a generalization of the FORCE flux (12) by considering convex averages of fluxes (10) and (11).

3.1. Convex averages

For our purpose, we first consider the model linear advection equation

$$\partial_t q + \lambda \partial_x q = 0, \quad \lambda: \text{ constant}. \tag{13}$$

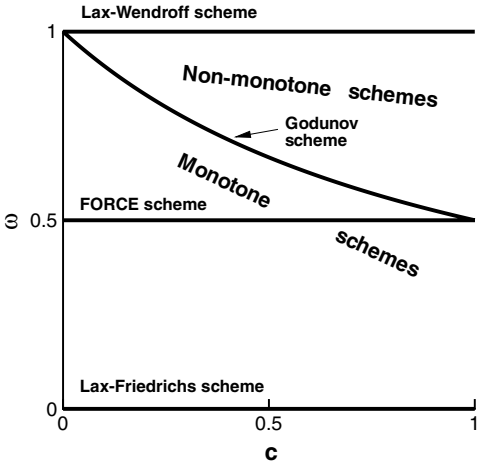

Fig. 1. Numerical fluxes as convex averages of the Lax-Friedrichs and Lax-Wendroff fluxes in the c–ω plane. Here c is Courant number and ω is a weight, whose constant values 0, $\frac{1}{2}$ and 1 reproduce the Lax-Friedrichs, FORCE and Lax-Wendroff fluxes; $\omega = \frac{1}{1+|c|}$ reproduces the Godunov upwind method.

The physical flux function is a linear function of the unknown q, namely $f(q) = \lambda q$. The corresponding conservative scheme is written as

$$q_i^{n+1} = q_i^n - \frac{\Delta t}{\Delta x}[f_{i+\frac{1}{2}} - f_{i-\frac{1}{2}}] \tag{14}$$

for which the Lax-Wendroff, Lax-Friedrichs and FORCE fluxes, respectively, are:

$$f_{i+\frac{1}{2}}^{\mathrm{lw}} = \frac{1}{2}(1+c)(\lambda q_i^n) + \frac{1}{2}(1-c)(\lambda q_{i+1}^n), \tag{15}$$

$$f_{i+\frac{1}{2}}^{\mathrm{lf}} = \frac{(1+c)}{2c}(\lambda q_i^n) - \frac{(1-c)}{2c}(\lambda q_{i+1}^n), \tag{16}$$

$$f_{i+\frac{1}{2}}^{\mathrm{force}} = \frac{(1+c)^2}{4c}(\lambda q_i^n) - \frac{(1-c)^2}{4c}(\lambda q_{i+1}^n), \tag{17}$$

where c is the CFL or Courant number $c = \frac{\lambda \Delta t}{\Delta x}$.

Now consider convex averages of the Lax-Friedrichs and the two-step Lax-Wendroff fluxes as follows:

$$f_{i+\frac{1}{2}}^{(\omega)} = \omega f_{i+\frac{1}{2}}^{\mathrm{lw}} + (1-\omega) f_{i+\frac{1}{2}}^{\mathrm{lf}} \tag{18}$$

with the weight ω satisfying $0 \leqslant \omega \leqslant 1$. When written in full, (18) reads

$$f_{i+\frac{1}{2}}^{(\omega)} = \frac{1}{2}(1+c)\left[\frac{-(1-c)\omega + 1}{c}\right](\lambda q_i^n) + \frac{1}{2}(1-c)\left[\frac{(1+c)\omega - 1}{c}\right](\lambda q_{i+1}^n). \tag{19}$$

In the c–ω plane of Fig. 1 we show special curves $\omega(c)$ that when substituted into (19) reproduce well-known numerical fluxes. For example, the bottom horizontal line with constant weight $\omega = 0$ gives the Lax-Friedrichs flux. The top horizontal line with constant weight $\omega = 1$ gives the Lax-Wendroff flux. For the constant weight $\omega = \frac{1}{2}$, we reproduce the FORCE flux (12) for non-linear systems (5) and the flux (17) for the linear advection equation (13).

3.2. The generalized FORCE flux: GFORCE

By comparing the coefficients of the flux (19) with those of the Godunov upwind flux

$$f_{i+\frac{1}{2}}^{\mathrm{GodU}} = \begin{cases} \lambda q_i^n & \text{if } \lambda > 0, \\ \lambda q_{i+1}^n & \text{if } \lambda < 0, \end{cases} \tag{20}$$

we obtain the Courant number dependent weight given by

$$\omega_g(c) = \frac{1}{1+|c|} \tag{21}$$

for which the convex average flux (19) reproduces identically the Godunov's upwind flux. For any constant value of the weight ω with $\omega \leqslant \omega \leqslant 1$ we have a 3-point scheme (14) whose coefficient of numerical dissipation is

$$\alpha = \frac{1}{2}\left[\frac{(1-c^2)(1-\omega)}{c}\right]\lambda\Delta x, \tag{22}$$

which varies linearly with ω, it is a maximum for the Lax-Friedrichs flux ($\omega = 0$) and zero for the Lax-Wendroff flux ($\omega = 1$).

The curve $\omega_g(c)$ divides the unit square of Fig. 1 into two subregions. The region associated with weights lying above the Godunov weight $\omega_g(c)$ contains non-monotone schemes and the region below $\omega_g(c)$ contains monotone schemes. The range of *constant* weights ω (no dependence on c), with $0 \leqslant \omega \leqslant \frac{1}{2}$, defines a sub-class of monotone schemes, with the FORCE flux (17) corresponding to the limiting case $\omega = \frac{1}{2}$, which is the scheme with the smallest numerical dissipation within the class, and thus the optimal scheme, for which no dependence on c (no upwind information) is required.

In order to improve upon the centred flux FORCE, that is, reduce its numerical dissipation further, we need to consider entering the region $\frac{1}{2} < \omega \leqslant 1$, within which all schemes (19) with constant weight ω are *non-monotone*; monotonicity is lost for the larger range of CFL numbers.

In resolving this problem we consider the following set:

$$T_g = \left\{(c,w) : 0 \leqslant c \leqslant 1 \quad \text{and} \quad \frac{1}{2} < \omega \leqslant \omega_g(c) = \frac{1}{1+|c|}\right\}. \tag{23}$$

This kind of triangular subregion in Fig. 1, with a curved *hypotenuse*, represents extra numerical dissipation to that of the FORCE flux, the optimal scheme in its class that makes no explicit use of wave propagation information. The upper boundary of T_g, given by (21), gives precisely the Godunov upwind scheme, the monotone scheme with the smallest coefficient of numerical dissipation, namely

$$\alpha_{\mathrm{god}} = \frac{1}{2}(1-|c|)\lambda\Delta x. \tag{24}$$

The main objective of this paper is to regain the region T_g, but without having to solve the Riemann problem, at least not in the conventional sense. We present two ways of disposing of the additional numerical dissipation represented by T_g and contained in the optimal centred method, FORCE. First we propose the numerical flux

$$\mathbf{F}_{i+\frac{1}{2}}^{\mathrm{GFORCE}} = \omega_g \mathbf{F}_{i+\frac{1}{2}}^{\mathrm{LW}} + (1-\omega_g)\mathbf{F}_{i+\frac{1}{2}}^{\mathrm{LF}}, \tag{25}$$

where ω_g has the form

$$\omega_g = \frac{1}{1+c_g}. \tag{26}$$

Here c_g is a prescribed Courant number coefficient, with $0 \leqslant c_g \leqslant 1$, from which a time step is computed, see Section 4. The flux (25) is called GFORCE, where **G** may be seen as short for Generalization of the FORCE flux or a special case of the Godunov flux; it is obvious that for the linear advection equation with constant coefficient (13) the proposed GFORCE flux (25) reproduces identically the Godunov's upwind flux (20), fully recovering the subregion T_g.

For non-linear systems, however, GFORCE does not reproduce the Godunov flux, that is, it does not fully recover T_g. In practice, nonetheless, GFORCE gives results that are comparable, and sometimes superior, to those of well established Godunov-type methods with incomplete Riemann solvers, such as the HLL approx-

imate Riemann solver [14]. The results of GFORCE are still inferior to those of the Godunov method used in conjunction with complete Riemann solvers. This is most evident for problems in which the resolution of intermediate waves is important. A further step in attempting to fully regain T_g for non-linear systems is offered by the MUSTA approach [34], the subject of the following section.

4. MUSTA fluxes

In the MUSTA multi-stage approach [34] the numerical flux $\mathbf{F}_{i+\frac{1}{2}}$ for the conservative scheme (6) is found by first approximating numerically the solution of the corresponding Riemann problem (7) to produce two *modified* states either side of the cell interface. This part is termed the predictor step. In the corrector step one obtains the sought intercell numerical flux by evaluating a numerical flux function at the two modified states of the predictor step. An improved version of the MUSTA original approach using the FORCE flux is given in [33].

4.1. The approach

Let us consider the Riemann problem (7). As the solution is self-similar we may pose the Cauchy problem on a d–τ plane of independent variables, where d denotes the spatial variable, associated with x, and τ denotes the temporal variable, associated with t. Then we approximate the solution of the Riemann problem

$$\left.\begin{aligned} &\partial_\tau \mathbf{Q} + \partial_d \mathbf{F}(\mathbf{Q}) = \mathbf{0}, \quad d \in (-\infty, \infty), \quad \tau > 0 \\ &\mathbf{Q}(d,0) = \begin{cases} \mathbf{Q}_i^n & \text{if } d < 0, \\ \mathbf{Q}_{i+1}^n & \text{if } d > 0 \end{cases} \end{aligned}\right\} \tag{27}$$

numerically, for which we generate a *separate*, independent mesh, called hereafter the *MUSTA mesh*.

Fig. 2 shows the correspondence between the cells i and $i+1$ of the computational mesh for (6) on the x–t plane and the MUSTA mesh on the d–τ plane. The d-axis is discretized into a number M of cells of regular size Δd, where M is a positive integer yet to be specified. Note that cells i and $i+1$ in (a) correspond, respectively, to cells 0 and 1 on the MUSTA mesh in (b), so that the intercell position $i+1/2$ in the scheme (6) corresponds to the interface 1/2.

The initial condition for the numerical problem on the MUSTA mesh is

$$\mathbf{Q}_l^{(0)} = \begin{cases} \mathbf{Q}_i^n & \text{if } l \leqslant 0, \\ \mathbf{Q}_{i+1}^n & \text{if } l \geqslant 1. \end{cases} \tag{28}$$

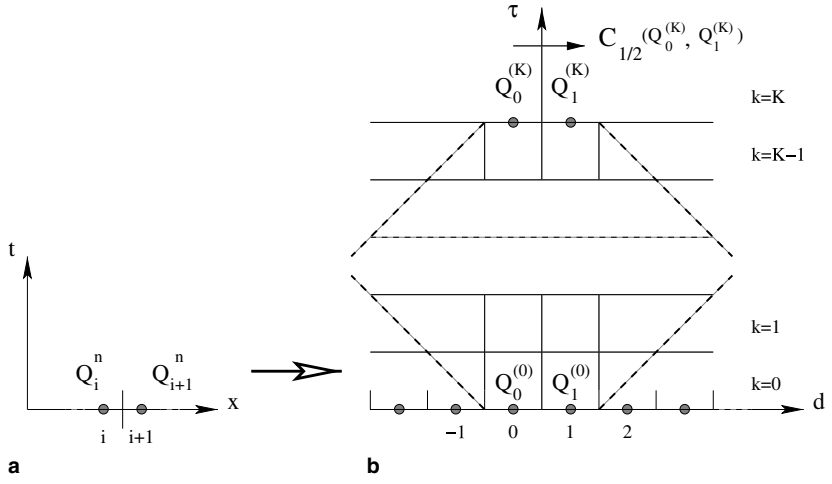

Fig. 2. The MUSTA approach. (a) Initial data $(\mathbf{Q}_i^n, \mathbf{Q}_{i+1}^n)$ in original computational mesh on x–t plane, (b) corresponding MUSTA mesh on d–τ plane. Sought numerical flux in (6) to be found by *resolving evolved data* $(\mathbf{Q}_0^{(K)}, \mathbf{Q}_1^{(K)})$.

The τ-time evolution of the problem (or multi-staging) is performed via the conservative scheme

$$\mathbf{Q}_l^{(k+1)} = \mathbf{Q}_l^{(k)} - \frac{\Delta\tau}{\Delta d}\left[\mathbf{P}_{l+\frac{1}{2}}^{(k)} - \mathbf{P}_{l+\frac{1}{2}}^{(k)}\right], \tag{29}$$

where $\Delta\tau$ is the *time step* in the *MUSTA mesh* and $\mathbf{P}(\mathbf{V}_L,\mathbf{V}_R)$ is a two-point monotone numerical flux for the *MUSTA mesh*, called the *predictor flux*, yet to be specified. Note that we are free to choose the spacing Δd on the MUSTA mesh. We usually take $\Delta d = 1$.

The MUSTA time step $\Delta\tau$ is computed as $\Delta\tau = C_{\text{musta}}\Delta d/S_{\text{musta}}^{(k)}$, where C_{musta} is the CFL coefficient, which depends on the specific predictor flux function $\mathbf{P}$ used on the MUSTA mesh. Note that C_{musta} is identical to c_g in Eq. (26). $S_{\text{musta}}^{(k)}$ is the maximum signal speed in the *MUSTA mesh* at stage k and depends on the particular hyperbolic system under consideration. After a prescribed number of stages K, which corresponds to a prescribed number of τ-time steps in the τ direction, the predictor procedure yields two new intercell states $\mathbf{Q}_0^{(K)}$ and $\mathbf{Q}_1^{(K)}$ on the *MUSTA mesh*. See Fig. 2(b).

For a sufficiently large number of stages and a convergent scheme (29) one would obtain an approximation to the solution of the Riemann problem (7) at two positions left and right close to the interface position, not at the interface itself. Thus in order to obtain a numerical flux at the interface itself we perform a *corrector stage*, whereby the evolved data $(\mathbf{Q}_0^{(K)}, \mathbf{Q}_1^{(K)})$ is *resolved* via a two-point, monotone numerical flux $\mathbf{C}(\mathbf{V}_L,\mathbf{V}_R)$, called the corrector flux. In this manner the sought intercell numerical flux $\mathbf{F}_{i+\frac{1}{2}}$ for use in the conservative scheme (6) is found thus

$$\mathbf{F}_{i+\frac{1}{2}}^{\text{MUSTA-K}} = \mathbf{C}_{1/2}(\mathbf{Q}_0^{(K)}, \mathbf{Q}_1^{(K)}). \tag{30}$$

Fig. 2 illustrates the MUSTA procedure for an arbitrary number of stages K.

To completely determine the numerical procedure on the MUSTA mesh we must make a choice for the predictor and corrector fluxes. This is discussed in Section 4.4. In practice we must also (i) choose a mesh, (ii) prescribe a number K of stages and (iii) specify numerical boundary conditions.

4.2. The MUSTA domain and boundary conditions

Numerical boundary conditions on the MUSTA mesh must be specified, for which we note that the computational domain is somewhat special. See Fig. 2(b). Given the fact that the Riemann-like initial condition extends the value $\mathbf{Q}_i^n$ to $-\infty$ and the value $\mathbf{Q}_{i+1}^n$ to ∞ we would need to apply special boundary conditions of the transmissive or radiating type, which would allow the unimpeded passage of waves through the boundaries. As reported in [34], the choice of a MUSTA domain of just two cells and the application of simple transmissive boundary conditions may lead to the loss of monotonicity of the resulting MUSTA numerical schemes, which is undesirable. See [34].

A possible, and very simple, approach is to select a MUSTA computational domain sufficiently large [33] so that for a prescribed number of stages K the waves emerging from the initial interface do not reach the numerical boundaries. In this manner one effectively avoids the application of boundary conditions, with the boundary fluxes being evaluated on the nearest cells in the interior of the computational domain. This approach would be computationally expensive, although it could be improved by choosing a fixed *MUSTA mesh* of precisely $M = 2K$ cells, assuming that one uses a CFL coefficient close to unity in (29), with the cell label l satisfying $-K \leqslant l \leqslant K$. Note that unnecessary computations are performed in the *regions of silence* not affected by the perturbations caused by the initial discontinuity. A more efficient version of this scheme starts the computations with a *MUSTA mesh* of 2 cells (0 and 1) and then adds one cell on either side per stage, resulting in a final mesh that has a V-like shape, leading to a reduction of the computational cost by a factor of two.

The procedure we adopt here is even more efficient, resulting in a saving factor of about four, relative to that in which a fixed mesh of $2K$ cells is used. Computations are performed on a stage-dependent domain that has the shape of a diamond, as suggested by the broken lines of Fig. 2(b). In this case the index l in (29) at the stage k satisfies

$$-l_Q(k) + 1 \leqslant l \leqslant l_Q(k), \tag{31}$$

where $l_Q(k)$ is the range for the conserved variable vector Q. In the algorithm there is also a range for the fluxes $\mathbf{P}_{l+\frac{1}{2}}^{(k)}$ in (29), denoted by $l_P(k)$, for which $-l_P(k) \leqslant l \leqslant l_P(k)$.

An algorithm in the form of a FORTRAN program for the MUSTA-1 scheme is included in the Appendix.

4.3. Example of a MUSTA scheme

The simplest MUSTA scheme is the one-stage scheme, or MUSTA-1, illustrated in Fig. 3. The initial data is prescribed in the domain of just two cells, namely $l = 0$ and $l = 1$. The boundary fluxes $\mathbf{P}^{(0)}_{-1/2}$ and $\mathbf{P}^{(0)}_{3/2}$, denoted by broken arrows in Fig. 3, are computed on the initial data, namely $\mathbf{P}^{(0)}_{-1/2} = \mathbf{F}(\mathbf{Q}^{(0)}_0)$ and $\mathbf{P}^{(0)}_{3/2} = \mathbf{F}(\mathbf{Q}^{(0)}_1)$. The only non-trivial flux is $\mathbf{P}^{(0)}_{1/2}$, which is shown by a full arrow in Fig. 3. Using (29) we evolve $\mathbf{Q}^{(0)}_0$ and $\mathbf{Q}^{(0)}_1$ as

$$\mathbf{Q}^{(1)}_0 = \mathbf{Q}^{(0)}_0 - \Delta\tau^{(0)}[\mathbf{P}^{(0)}_{1/2} - \mathbf{P}^{(0)}_{-1/2}], \quad \mathbf{Q}^{(1)}_1 = \mathbf{Q}^{(0)}_1 - \Delta\tau^{(0)}[\mathbf{P}^{(0)}_{3/2} - \mathbf{P}^{(0)}_{1/2}]. \tag{32}$$

Here $\Delta\tau^{(0)}$ is the size of the stable *time step* calculated on the initial data $(\mathbf{Q}^{(0)}_0, \mathbf{Q}^{(0)}_1)$ and the *spacing* has been set as $\Delta d = 1$.

As $K = 1$, the multi-staging is complete and the sought numerical flux is obtained by applying a corrector flux $\mathbf{C}(\mathbf{V}_L, \mathbf{V}_R)$ to the evolved data $\mathbf{Q}^{(1)}_0$ and $\mathbf{Q}^{(1)}_1$, namely

$$\mathbf{F}^{\text{MUSTA-1}}_{i+\frac{1}{2}} = \mathbf{C}_{1/2}(\mathbf{Q}^{(1)}_0, \mathbf{Q}^{(1)}_1). \tag{33}$$

A FORTRAN program for GMUSTA-1 is given in the Appendix.

4.4. Predictor and corrector fluxes

In choosing the predictor $\mathbf{P}(\mathbf{V}_L, \mathbf{V}_R)$ and corrector $\mathbf{C}(\mathbf{V}_L, \mathbf{V}_R)$ intercell fluxes for the MUSTA mesh, two properties are sought: (a) simplicity and (b) generality. Given that the MUSTA schemes require a few flux evaluations, simplicity, that hopefully results in computational efficiency, is required. The sought generality concerns the possibility of applying the MUSTA schemes to any hyperbolic system determined by the pair of vectors (**Q**,**F**), particularly for systems that do not have a known Riemann solver. Two families of MUSTA schemes emerge, as discussed below.

The most general MUSTA schemes utilize a simple flux both for the predictor $\mathbf{P}(\mathbf{V}_L, \mathbf{V}_R)$ and the corrector $\mathbf{C}(\mathbf{V}_L, \mathbf{V}_R)$ fluxes. The simplest productive choice of a symmetric flux is the FORCE flux (12) [34,33]. A more elaborate choice for predictor and corrector fluxes is the GFORCE (25) presented here, which requires a minimum of local wave propagation information, similarly to the Rusanov flux [29]. The MUSTA results shown in this paper are based on the GFORCE flux used both as a predictor and a corrector. The resulting MUSTA schemes are indeed very general and are *upwind*. The solution of the corresponding Riemann problem has been approximated numerically via the multi-staging procedure.

A particular class of MUSTA methods, recently proposed in [40], uses the MUSTA predictor stage (s) to produce evolved initial conditions, which in the corrector stage are taken as the initial data for a *simple* linearized Riemann problem, whose solution may be obtained in closed form. For this variant of MUSTA one requires the complete eigenstructure of the system, which restricts its range of applicability.

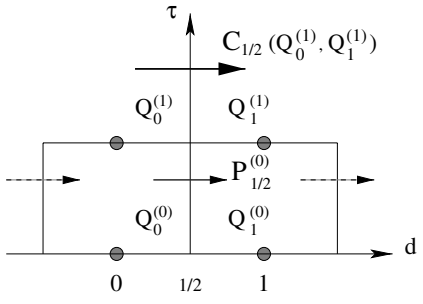

Fig. 3. Illustration of the one-stage MUSTA-1 scheme ($K = 1$).

4.5. Choice of the number of stages K

A MUSTA-K requires the choice of the number of multi-stages K, see Fig. 2. With $K = 0$ one obtains the original scheme associated with the chosen predictor flux. In theory, for a very large number of stages, under the assumption that the predictor flux gives a convergent scheme, the resulting MUSTA-K scheme should be close to the Godunov scheme, the reference first-order method. The experience of exhaustive testing for non-linear systems in one and multiple space dimensions indicates that the solution of the MUSTA-K scheme converges rapidly to the solution of the Godunov scheme used in conjunction with the exact Riemann solver. This observed convergence takes place without imposing convergence of the MUSTA multi-staging procedure at the predictor stage, see Fig. 2(b). The choice $K = 1$ is recommended for practical applications; the gains in using GMUSTA-2 and GMUSTA-3 does probably not justify the extra expense. The (limited) experience with the EVILIN variant [40], also suggests that it is sufficient to take one predictor stage, followed by the corrector step via a simple linearization. These observations will be supported by the numerical experiments shown in Section 5.

4.6. Properties of the MUSTA schemes

4.6.1. Relation to Godunov's flux

As already remarked, the GFORCE flux (25) reproduces identically the Godunov upwind flux (20) for the linear advection equation with constant coefficient (13). Here we note that this property also holds for the MUSTA schemes based on the GFORCE flux (25) used as predictor and corrector, when applied to (13). This is easily proved for an arbitrary number of stages K. Table 1 illustrates the evolution of the initial data states q_L, q_R in the MUSTA multi-staging procedure. For a positive wave speed λ the left state q_L remains unaltered, while the right state q_R changes at every stage. However, the relevant intercell flux $p^{(k)}_{1/2}$ remains constant and equal to that of the Godunov's upwind scheme.

As a consequence of the fact that MUSTA-K, for any number of stages K, reproduces the Godunov schemes identically for the linear advection equation with constant coefficient (13), the MUSTA-K schemes inherit a number of desirable properties, as seen below.

For the linear advection equation with constant coefficient (13), the scheme is *monotone* and has the smallest truncation error within the class of monotone schemes. The leading term of the truncation error has coefficient as given by (24).

4.6.2. Linear stability in multiple dimensions

Regarding stability, for the linear advection equation with constant coefficient (13) the scheme has *linear stability* condition

$$0 < |c| \leqslant 1. \tag{34}$$

The schemes presented here can be extended to solve multi-dimensional problems in a straightforward manner. Let us consider the model linear advection equation with constant coefficients in three space dimensions

$$\frac{\partial}{\partial t} q + \frac{\partial}{\partial x} f(q) + \frac{\partial}{\partial y} g(q) + \frac{\partial}{\partial z} h(q) = 0, \quad f = \lambda_1 q, \quad g = \lambda_2 q, \quad h = \lambda_3 q, \tag{35}$$

Table 1
The MUSTA flux for linear advection using the GFORCE scheme as predictor and corrector, for 3 stages. At each stage, the Godunov upwind flux is reproduced identically, see column 5

k	$q^{(k)}_0$	$q^{(k)}_1$	$p^{(k)}_{-1/2}$	$p^{(k)}_{1/2}$	$p^{(k)}_{3/2}$
0	q_L	q_R	λq_L	λq_L	λq_R
1	q_L	$cq_L + (1-c)q^{(0)}_1$	λq_L	λq_L	$\lambda q^{(1)}_1$
2	q_L	$cq_L + (1-c)q^{(1)}_1$	λq_L	λq_L	$\lambda q^{(2)}_1$
3	q_L	$cq_L + (1-c)q^{(2)}_1$	λq_L	λq_L	$\lambda q^{(3)}_1$

where the coefficients λ_1, λ_2, λ_3 are constant. Without loss of generality they are assumed positive. We consider unsplit schemes of the form (3), which for 3D Cartesian volumes of dimensions $\Delta x \times \Delta y \times \Delta z$ read

$$q_{ijk}^{n+1} = q_{ijk}^{n} - \frac{\Delta t}{\Delta x}(f_{i+1/2,jk} - f_{i-1/2,jk}) - \frac{\Delta t}{\Delta y}(g_{ij+1/2,k} - g_{ij-1/2,k}) - \frac{\Delta t}{\Delta z}(h_{ijk+1/2} - h_{ijk-1/2}). \tag{36}$$

The analysis of the *linear stability* for the schemes in two and three space dimensions is algebraically intractable. Using a numerical procedure [5,41], it is possible to obtain a reliable indication of the stability regions for the schemes, which for the three-dimensional case can be approximately written as

$$c_x + c_y + c_z \leqslant 1, \tag{37}$$

where $c_x = \lambda_1 \Delta t/\Delta x$, $c_y = \lambda_2 \Delta t/\Delta y$ and $c_z = \lambda_3 \Delta t/\Delta z$ are directional Courant numbers.

Regarding the extension of the MUSTA-K schemes to two- and three-dimensional hyperbolic systems we consider only the straightforward un-split form of finite volume methods, such as (3) or (36), whereby the MUSTA-K or other fluxes at the appropriate integration points, are the simple one-dimensional fluxes in the normal direction to the interface at the appropriate integration point. No attempt is made here to apply special procedures, such as pre-evolution of the initial conditions in the transverse direction, as done for example in [2], in order increase the stability region, for instance. See also [5,43]. Under such framework, non-upwind numerical fluxes, such Lax-Friedrichs and FORCE, are unconditionally unstable [41].

4.6.3. Relation to centred schemes

The MUSTA schemes of this paper and the well-known family of centred schemes [19,25,38,41,21] share the common property of being capable of solving hyperbolic problems for which Riemann solvers constructed in the classical manner are not available. Moreover, the zero-stage MUSTA scheme is identical to the scheme used as a predictor/corrector in the MUSTA scheme. For example, the zero-stage MUSTA constructed on the basis of the FORCE flux reproduces identically the FORCE scheme, and as remarked in [4], the FORCE scheme can be interpreted as a single-step, conservative, non-staggered grid version of the first-order mode of the scheme in [25].

We emphasize however that the MUSTA flux of one stage or more, is upwind, even when using non-upwind predictor/corrector fluxes. As a consequence, when applied to multiple space dimensions in the straightforward un-split manner (36), the proposed MUSTA schemes inherit the linear stability properties of the Godunov's upwind method. We remind the reader that known first-order symmetric schemes are unconditionally unstable under this framework [41].

5. Applications of GFORCE and GMUSTA

An attractive feature of the numerical fluxes presented in this paper is the ease with which one can solve complicated problems. As seen in (4) the computation of the numerical flux only involves evaluation of the normal flux and in the present approach this is done without having to solve directly the Riemann problem (7). This means that the method can be applied to general hyperbolic systems in conservation form. The restriction imposed by a particular hyperbolic system enters in the estimation of a local maximum signal speed to compute a stable time step for the scheme. We assume that sufficient information on the eigenvalues of the system for this purpose is available; for very complicated systems such information will probably be available by numerical means. Therefore, such procedure can also be applied in the MUSTA mesh to estimate the speeds $S_{\text{musta}}^{(k)}$ in the computation of the numerical flux, see (29). Here, we assess the proposed methods in terms of various test problems for non-linear systems in one and two space dimensions.

5.1. The Euler equations for compressible materials

The non-linear time-dependent one-dimensional Euler equations are

$$\left.\begin{aligned} &\partial_t \mathbf{Q} + \partial_x \mathbf{F}(\mathbf{Q}) = \mathbf{0}, \\ &\mathbf{Q} = \begin{bmatrix} \rho \\ \rho u \\ E \end{bmatrix}; \quad \mathbf{F}(\mathbf{Q}) = \begin{bmatrix} \rho u \\ \rho u^2 + p \\ u(E+p) \end{bmatrix}. \end{aligned}\right\} \tag{38}$$

Here ρ, u, p and E are density, particle speed, pressure and total energy, given by

$$E = \rho\left(\frac{1}{2}u^2 + e\right), \tag{39}$$

where e is the specific internal energy. The eigenvalues of (38) are easily found to be

$$\lambda_1 = u - a, \quad \lambda_2 = u, \quad \lambda_3 = u + a, \tag{40}$$

where a is the speed of sound in the material, which depends on the appropriate equation of state for the material.

The Euler equations (38), that govern the dynamics of wave propagation in a material, are supplemented by a thermodynamics statement as to the nature of that material, via a caloric equation of state (EOS), which is a functional (non-differential) relationship between three variables. A popular choice is the trio ρ, p and e. Another choice is furnished by the specific volume $v = 1/\rho$, pressure p and specific entropy s. The particular form of the equation of state determines the form of the sound speed a. Three forms of the equation of state and the corresponding expressions for the speed of sound are:

$$\left.\begin{aligned} &p = p(\rho, e), \quad a = \sqrt{\tfrac{p}{\rho^2}p_e + p_\rho}, \\ &e = e(\rho, p), \quad a = \sqrt{\tfrac{p}{\rho^2 e_p} - \tfrac{e_\rho}{e_p}}, \\ &p = p(v, s), \quad a = \sqrt{-v^2 p_v}, \end{aligned}\right\} \tag{41}$$

where subscripts denote partial derivatives.

For hyperbolicity of the Euler equations (38) one requires the sound speed to be real, which from (41) results in the condition

$$p_v = -e_{vv}(v, s) < 0. \tag{42}$$

A further restriction on the EOS results from imposing that the acoustic characteristic fields associated with the eigenvalues $\lambda_1 = u - a$ and $\lambda_3 = u + a$ be *genuinely non-linear*. This is usually known as the *convexity* condition for the Euler equations and may be expressed as

$$e_{vvv}(v, s) \neq 0. \tag{43}$$

More general materials not obeying the convexity assumption may also be considered, in which case, complex wave patterns may occur, such as rarefaction shock waves and composite waves. See [24].

Upwind Godunov-type methods require the solution of the Riemann problem for (38) along with a general equation of state (41). This can be costly, complex or impossible. For background see the works of Colella and Glaz [6], Glaister [9], Menikoff and Plohr [24] and Quartapelle et al. [27], amongst others. The methods of this paper do not require such solution and are directly applicable.

As an example we consider a simple generalization of the ideal gas equation of state, the so-called *covolume equation of state*,

$$e = \frac{p(1 - b\rho)}{\rho(\gamma - 1)}, \quad a = \sqrt{\frac{\gamma p}{(1 - b\rho)\rho}}, \tag{44}$$

where γ is the ratio of specific heats (assumed constant) and b is called the *covolume*, which in SI units has dimensions of $\mathrm{m}^3\,\mathrm{kg}^{-1}$. The conventional ideal gas case is obtained from (44) with $b = 0$. Equation of state (44) applies to dense gases at high pressure, for which the volume occupied by the molecules themselves is no longer negligible. There is therefore a reduction in the volume available to molecular motion. Sometimes,

this equation is also called the Noble–Abel equation of state. In the study of propulsion systems, gaseous combustion products at very high densities are reasonably well described by the covolume equation of state. In its simplest version, the covolume b is a constant and is determined experimentally or from equilibrium thermochemical calculations. For an exact Riemann solver see [35].

5.2. Euler numerical examples

Here we assess the performance of the proposed MUSTA methods for four test problems for the time-dependent one-dimensional Euler equations, three for ideal gases and one for covolume gases in a problem with moving boundaries.

Test 1: Low density flow. We solve the one-dimensional Euler equations for an ideal gas with $\gamma = 1.4$ in the domain $[0,1]$. The initial condition consists of two constant states separated by a discontinuity positioned at $x = 1/2$. To the left of the discontinuity the initial values for density, velocity and pressure are $\rho_L = 1.0$, $u_L = -2.0$, $p_L = 0.4$ and to the right of the discontinuity they are $\rho_R = 1.0$, $u_R = 2.0$, $p_R = 0.4$. The purpose of this test problem is to assess the performance of the methods proposed in this paper for computing *low-density flows*, for which it is well known that linearized Riemann solvers, for example, fail [8], unless adhoc fixes are implemented.

Computed results for density and velocity are shown in Fig. 4, computed with the GMUSTA-1 scheme on a mesh of 100 cells and a CFL coefficient of 0.9. The exact solution (full line) is also shown, for comparison. The results are satisfactory, in particular for the velocity. We remark that for this test problem, even non-linear complete Riemann solvers, such as HLLC, do not give an accurate solution for the velocity in the middle region of stationary flow. See results of Chapter 10 of [39]. Computed results with GMUSTA-2 and GMUSTA-3 are very close to those displayed in Fig 4 and are omitted. We observe convergence of the GMUSTA-K schemes to the solution obtained with the Godunov method in conjunction with the exact Riemann solver (the reference solution); solutions for $K = 1$ and $K = 2$ are already very close to the reference solution, which suggests that GMUSTA-1 is a scheme that could be used in practice.

Test 2: Transonic flow. We solve the one-dimensional Euler equations for an ideal gas with $\gamma = 1.4$ in the domain $[0,1]$. The initial condition consists of two constant states separated by a discontinuity positioned at $x = 0.3$. To the left of the discontinuity the initial values for density, velocity and pressure are $\rho_L = 1.0$, $u_L = 0.75$, $p_L = 1.0$ and to the right of the discontinuity they are $\rho_R = 0.125$, $u_R = 0.0$, $p_R = 0.1$. The purpose of this test problem is to assess the performance of the methods proposed in this paper for computing transonic flows, for which it is well known that linearized Riemann solvers fail, unless adhoc entropy fixes are implemented.

Computed results for density and velocity are shown in Fig. 5 using the GMUSTA-1 scheme on a mesh of 100 cells and a CFL coefficient of 0.9. For comparison, we also show the exact solution (line) and the numerical solution obtained with the Godunov method in conjunction with the exact Riemann solver. We note that for the shock and the contact waves the numerical results from GMUSTA-1 and the Godunov method with the exact Riemann solver are virtually indistinguishable. At the sonic point the GMUSTA-1 solution is very smooth and more accurate than that of the Godunov scheme with the exact Riemann solver, but it is less accurate near the head and tail of the rarefaction. We note that the MUSTA approach does not require special treatment of sonic points and yet good results are obtained automatically for the class of problems with sonic points.

Test 3: Blast wave interaction. We solve the one-dimensional Euler equations for an ideal gas with $\gamma = 1.4$ in a domain $[0,1]$. The initial condition [47] consists of constant density $\rho = 1$, constant velocity $u = 0$ and a discontinuous distribution of pressure: $p_L = 1000$ in $[0, 1/10]$, $p_M = 0.01$ in $(1/10, 9/10]$ and $p_R = 100$ in $(9/10, 1]$. For a detailed discussion on the solution of this problem see [47]. The purpose of this test is to assess the robustness and accuracy of the proposed methods for resolving very strong shock waves and multiple wave–wave and wave–boundary interactions. Since the work of Woodward and Colella [47] it has become standard to solve this problem on a mesh of 3000 cells and display results at the output time $t = 0.038$.

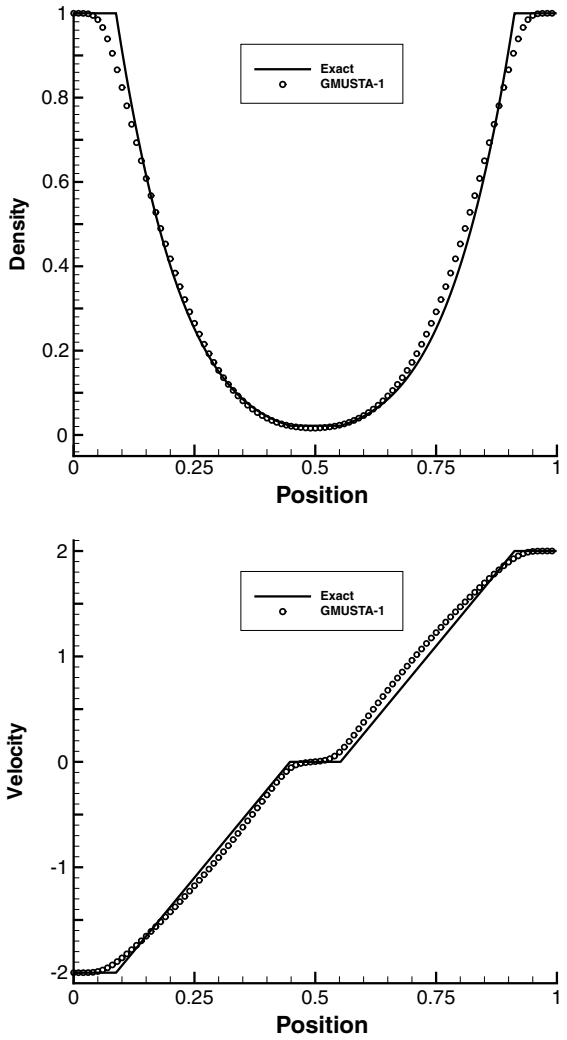

Fig. 4. *Test 1: Low density flow*. Numerical (symbols) and exact (line) solutions at time $t = 2.0$. Method used: GMUSTA-1 on mesh of 100 cells and CFL = 0.9.

In Fig. 6 we summarize some of the computations we have performed for this test problem, zooming into the critical region, where the largest differences between schemes are observed. First we note that the results of GMUSTA-1 and those of the Godunov method with the exact Riemann solver (our reference solution) are virtually indistinguishable. For comparison, we also show the results of the Lax-Friedrichs, FORCE, GFORCE schemes. It is seen that GFORCE is clearly more accurate than the other simple methods. Calculations omitted here show that GFORCE is even more accurate than incomplete Riemann solvers, such as the HLL approximate Riemann solver [14].

Test 4: Lagrange's problem with covolume. The Lagrange's problem is a test for both Euler solvers with the covolume equation of state (44) as well as for testing moving boundary schemes. The problem consists of a tube of constant, circular cross-sectional area with a combustion chamber at the left end, filled with stationary combustion products at high density and pressure. At the right-hand end of the combustion chamber is the base of a piston of a given mass, assumed to occupy the full cross-sectional area of the tube, so that the gases are sealed. See Table 2. A theoretical solution to this problem was obtained by Love and Pidduck [23], and Table 3 gives this for 10 values of time.

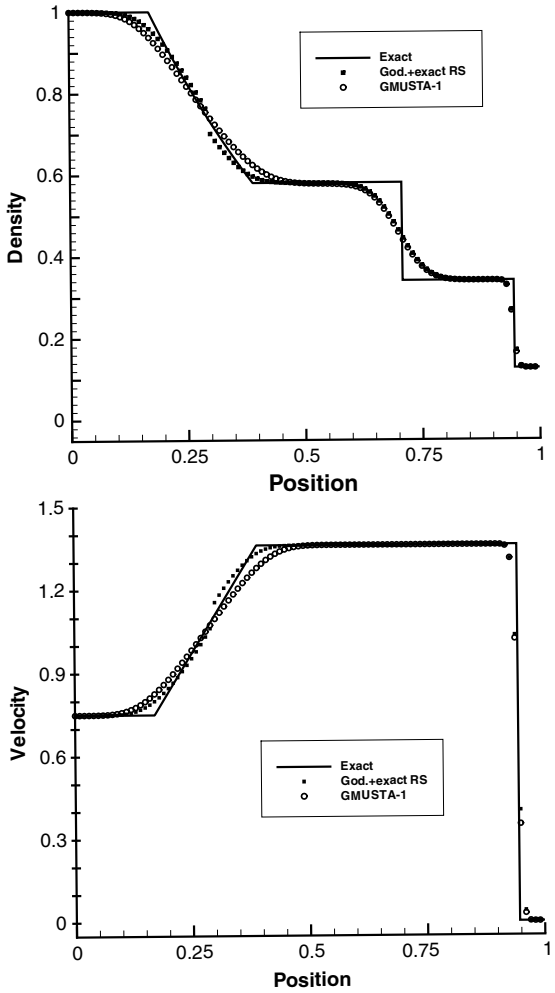

Fig. 5. *Test 2: Transonic flow*. Numerical (symbols) and exact (line) solutions at time $t = 2.0$. Methods used: GMUSTA-1 and Godunov with exact Riemann solver, on mesh of 100 cells and CFL = 0.9.

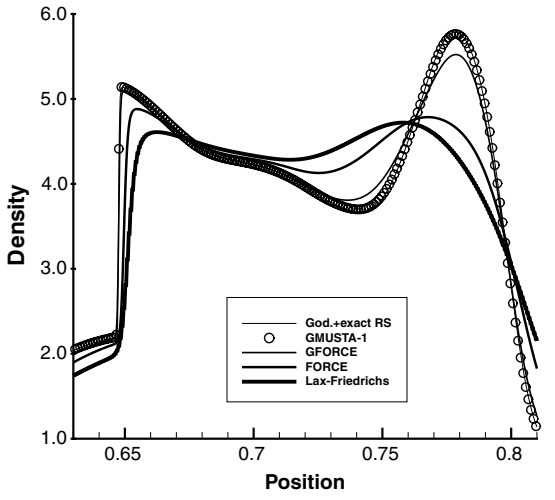

Fig. 6. *Test 3: Blast wave interaction*. Numerical solutions in zoomed region for density at time $t = 0.038$ using a mesh of 3000 cells and CFL = 0.9. Methods used: Godunov with the exact Riemann solver, GMUSTA-1, GFORCE, FORCE and Lax-Friedrichs.

Table 2
Data for the Lagrange's problem

Tube total length (m)	7.698
Tube radius (m)	0.075
Combustion chamber length (m)	1.698
Initial gas density in chamber (kg/m^3)	400.0
Initial gas speed in chamber (m/s)	0
Initial gas pressure in chamber (MPa)	621.0
Ratio of specific heats	11/9
Covolume (m^3/kg)	0.001
Total mass of piston (kg)	50

Table 3
Theoretical solution for the Lagrange's problem [23]

Time, ms	Piston base position	Piston speed	Breech pressure	Piston base pressure
0.4772	1.72165	99.64	621.06	554.17
0.9544	1.78965	187.70	621.06	499.84
1.4785	1.91165	275.40	507.10	451.01
2.1170	2.11965	371.80	408.84	402.27
2.8980	2.45165	466.20	325.19	291.26
3.8590	2.94065	550.40	255.95	212.84
5.1540	3.71865	632.50	169.46	150.53
7.1370	5.05365	718.30	106.50	101.10
10.2300	7.41665	801.30	63.74	57.04
10.5800	7.69765	807.70	60.88*	54.19

Value * obtained from interpolation procedure using a reference numerical solution with the WAF scheme [36].

At time $t = 0$ one assumes instantaneous combustion in the chamber and the piston is free to move under the action of the high pressure. At time $t = 10.58$ ms the base of the piston leaves the end of the tube at $x = 7.698$ m at an exit speed of $V = 807.70$ m/s. Fig. 7 shows results, as functions of time, for the piston base position, the piston speed, the pressure at the centre of the tube at $x = 0$ (the breech), and the pressure at the base of the piston. The numerical solution (full line) is compared with the theoretical solution (symbols) given in Table 3. The numerical results were obtained from a TVD extension of the MUSTA scheme, starting the computations with an initial mesh of $M = 100$ cells and then adding *cut cells* as the computational domain was enlarged due to the travelling of the piston towards the exit of the tube. As seen in Fig. 7, the agreement between the numerical and the theoretical solution is very satisfactory.

We have also solved this problem using the WAF method [36] in conjunction with the exact Riemann solver, using the WAF method with the HLLC Riemann solver [45] and using the Random Choice Method [37], obtaining similar results to those reported here. The comparison of results is omitted.

5.3. One-dimensional ideal magnetohydrodynamics

We solve the one-dimensional MHD equations:

$$\left.\begin{aligned} &\partial_t \mathbf{Q} + \partial_x \mathbf{F}(\mathbf{Q}) = 0, \\ &\mathbf{Q} = \begin{bmatrix} \rho \\ \rho u \\ \rho v \\ \rho w \\ E \\ B_y \\ B_z \end{bmatrix}, \quad \mathbf{F} = \begin{bmatrix} \rho u \\ \rho u^2 + p_T - B_x^2 \\ \rho uv - B_x B_y \\ \rho uw - B_x B_z \\ (E + p_T)u - B_x(uB_x + vB_y + wB_z) \\ B_y u - B_x v \\ B_z u - B_x w \end{bmatrix}, \end{aligned}\right\} \tag{45}$$

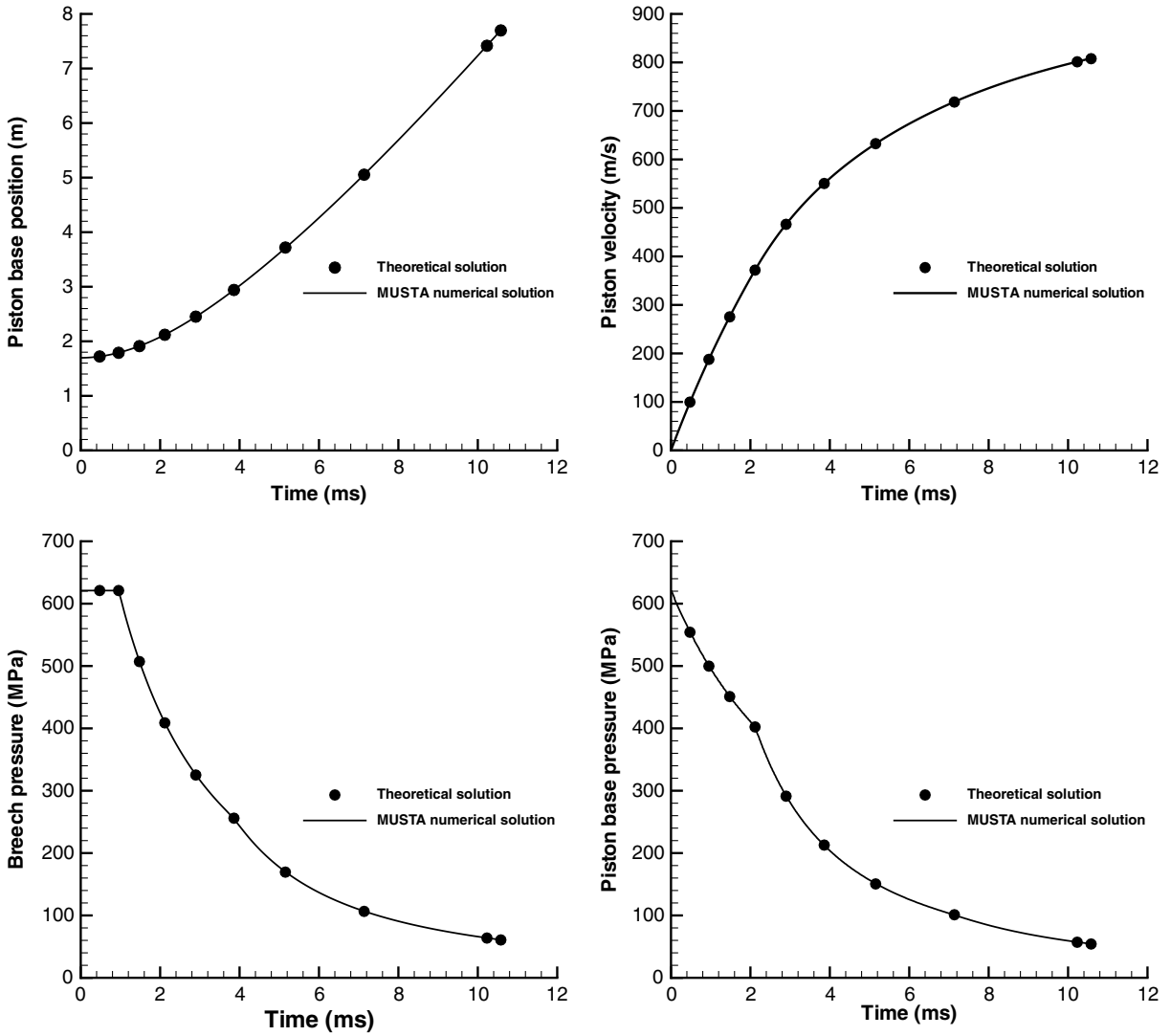

Fig. 7. *Test 4: Lagrange's problem with covolume*. Numerical (line) and theoretical (symbol) solution as function of time for piston base position, piston speed, pressure at breech and pressure at the base of the piston.

where $\mathbf{B} = (B_x, B_y, B_z)$ is the magnetic field,

$$p_T = p + \frac{1}{2}\mathbf{B}^2, \quad E = \frac{p}{(\gamma - 1)} + \frac{1}{2}\rho(u^2 + v^2 + w^2) + \frac{1}{2}\mathbf{B}^2, \tag{46}$$

p is the gasdynamical pressure, ρ is density, E is total energy and u, v, w are velocity components.

The one-dimensional MHD system is hyperbolic with the eigenvalues given by

$$\lambda_1 = u - c_\mathrm{f}, \quad \lambda_2 = u - c_\mathrm{A}, \quad \lambda_3 = u - c_\mathrm{s}, \quad \lambda_4 = u, \quad \lambda_5 = u + c_\mathrm{s}, \quad \lambda_6 = u + c_\mathrm{A}, \quad \lambda_7 = u + c_\mathrm{f}.$$

Here c_f, c_s are fast and slow magnetoacoustic velocities, c_A is the Alfven velocity.

We solve the Riemann problem for (45) with the parameters corresponding to the first test problem of Brio and Wu [3]. The computational domain is the interval $[-0.5,0.5]$, the ratio of specific heats is set to $\gamma = 2$. The initial conditions are as follows:

$$B_x = 0.75, \quad u = v = w = 0, \quad (\rho, p, B_y, B_z) = \begin{cases} (1.0, 1.0, +1.0, 0.0) & x < 0, \\ (0.125, 0.1, -1.0, 0.0) & x > 0. \end{cases} \tag{47}$$

We obtain a reference solution of (45) with the initial data (47) by applying the GMUSTA scheme on the very fine mesh of 10,000 cells. Comparing this reference solution with those reported in the current literature [3,16,17], we observe that a structure of the solution accepted as correct is obtained, which consists of a left travelling fast rarefaction wave, an intermediate shock and slow rarefaction wave as well as a right-travelling contact discontinuity, a slow shock and a fast rarefaction wave. The left travelling intermediate shock and the slow rarefaction wave form a feature that has been termed *compound wave* in the literature. Generally speaking the outlined structure of the solution is not stable with respect to tangential disturbances. If the complete three-dimensional MHD system is solved and the flow contains tangential disturbances, the so-called compound wave will decay and a different structure of the solution will be observed. See [1,17] for a more detailed discussion. For the one-dimensional system (45), however, the structure of the solution outlined above, is accepted as correct.

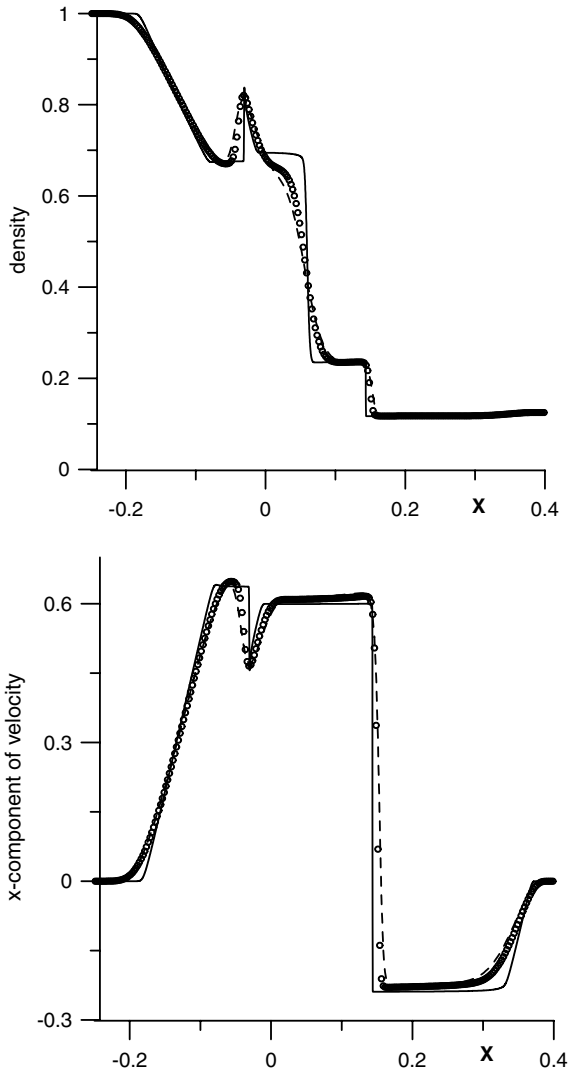

Fig. 8. *Brio and Wu MHD test problem.* GFORCE (dashed line) and GMUSTA-1 (symbols) results with CFL = 0.9 and 400 cells. Reference solution shown by full line.

Figs. 8 and 9 show computed results using the schemes presented in this paper using a mesh of 400 cells and a CFL coefficient CFL = 0.9. The GFORCE results are shown by the dashed line, the GMUSTA-1 results are shown by symbols and the reference solution is shown by the full line. We consider both numerical schemes to give satisfactory results, all main features of the solution are captured. As expected, the GMUSTA-1 results are more accurate than the GFORCE results, particularly for the contact wave.

For comparison with other simple methods, we have also computed the solution using the Lax-Friedrichs scheme and the FORCE scheme, which is algebraically equivalent to the two-step staggered grid Lax-Friedrichs method. The results presented in Fig. 10 for CFL = 0.9 show that the schemes of this paper are significantly more accurate, for all waves in the solution.

Moreover, as one would expect from the analysis of Fig. 1, the observed difference in accuracy increases for small Courant numbers. Fig. 11 shows a comparison of solutions for CFL = 0.2 and 400 cells. Large differences are observed. The two centred methods are badly affected by small CFL numbers. The significant improvement from Lax-Friedrichs to GFORCE and GMUSTA, specially for small CFL

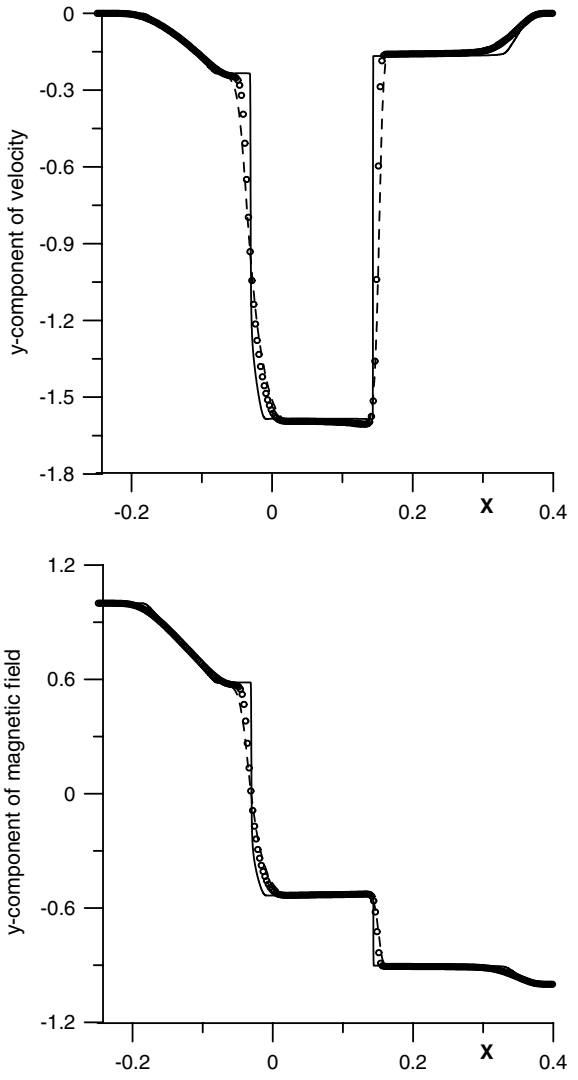

Fig. 9. *Brio and Wu MHD test problem.* GFORCE (dashed line) and GMUSTA-1 (symbols) results with CFL = 0.9 and 400 cells. Reference solution shown by full line.

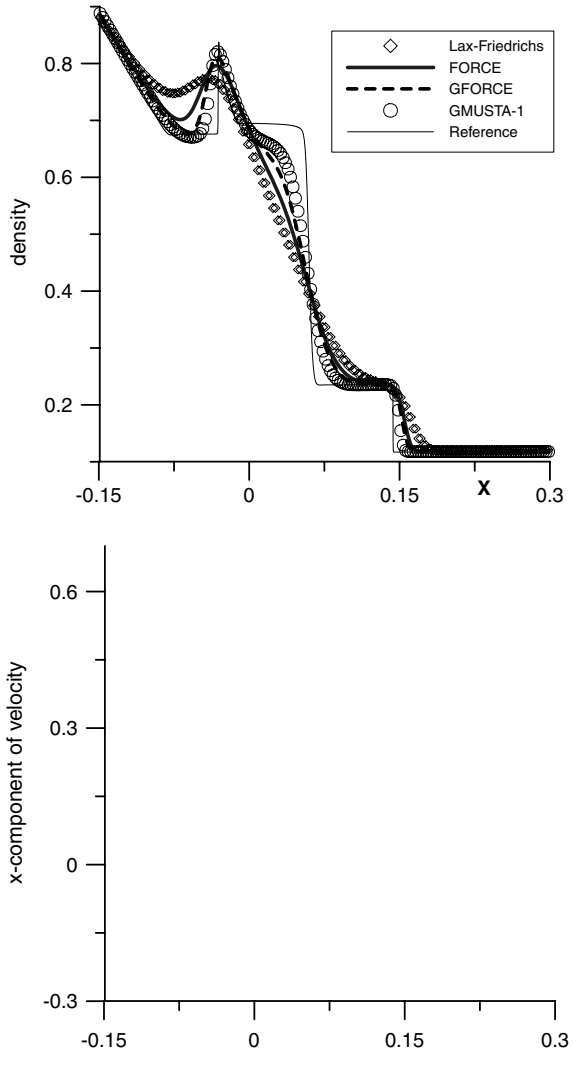

numbers, is explained by the discussion of Section 3.2, the local truncation error of the present schemes does not depend on the reciprocal of the time step. As a result, the accuracy of the GFORCE scheme, and thus GMUSTA, does not degrade much for small Courant numbers.

5.4. Multiple space dimensions and high order

The numerical fluxes proposed in this paper can be used directly in *unsplit, or simultaneous updating* finite volume schemes of the form (3), see also (36). The present schemes can also be used in the frame of discontinuous Galerkin approaches to obtain schemes of higher order of accuracy, along with various ways of constructing non-oscillatory versions of the schemes. In their simplest form, the resulting multi-dimensional schemes use the appropriate one-dimensional fluxes in the direction normal to the cell interface at the appropriate integration point. In this framework, any existing finite volume code based on some Riemann solver can be easily modified by replacing the numerical flux by the GMUSTA flux of this paper.

5.4.1. High-order WENO methods

The GMUSTA fluxes can be used to construct schemes of very high order of accuracy in space and time. Here we illustrate this in the frame of WENO schemes with Runge–Kutta time stepping, as applied to the two-dimensional Euler equations for ideal gases. We use GMUSTA as the building block in the state-of-art weighted essentially non-oscillatory (WENO) schemes. For a detailed description of finite-volume WENO schemes in two space dimensions see [30] and references therein and [31] for the three-dimensional extension.

In the WENO–GMUSTA scheme the evaluation of the numerical flux consists of two steps. First the spatial integrals over cell faces are discretized by using a certain Gaussian quadrature. In this paper we use the two-point quadrature. Next, for each quadrature point the standard WENO reconstruction procedure provides left and right boundary extrapolated values. The resulting discontinuity is resolved by means of the so-called numerical flux, which is a two-point function, also called the building block of the scheme. Different monotone numerical fluxes can be used as the building block. For example, Shi and Shu [30] use the Rusanov flux as the building block. In this paper, we replace the conventional two-point numerical flux used as the

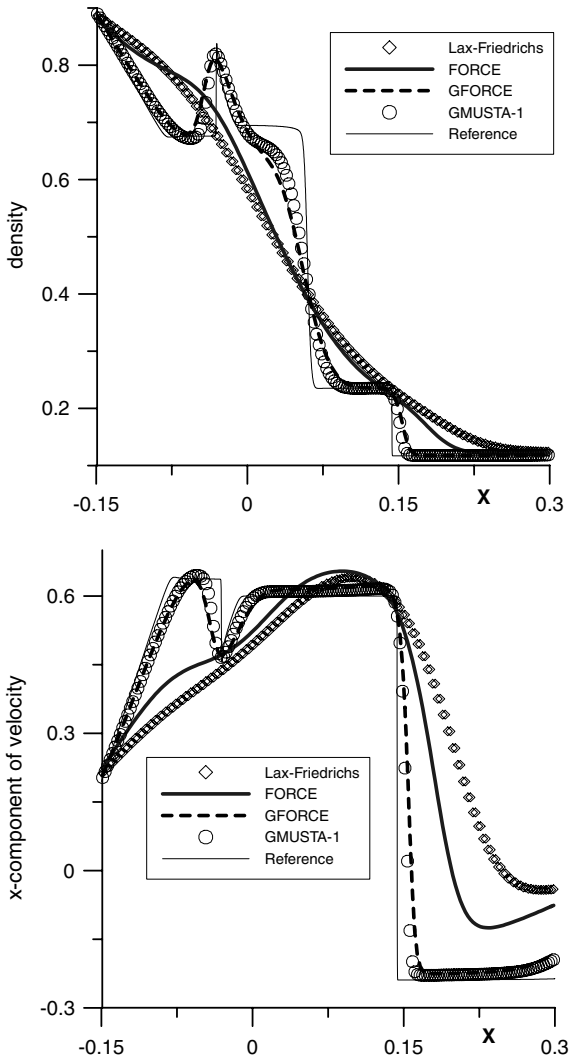

Fig. 11. *Brio and Wu MHD test problem.* Numerical solutions with CFL = 0.2 and 400 cells. Reference solution shown by full line.

building block in WENO (e.g. Rusanov or HLLC flux) by the two-point GMUSTA flux and denote the resulting scheme as the WENO–GMUSTA scheme.

In all examples of this section, fifth-order spatial reconstruction and third-order time integrations are used, see [30,31] for details. We note that in two space dimensions the variant of the WENO scheme from [31] is different from that of [30] in that it uses a two-point Gaussian quadrature instead of a three point quadrature.

5.4.2. Computation of double Mach reflection

We solve the two-dimensional compressible Euler equations for an ideal gas in a rectangular domain. The formulation of the Mach reflection problem, computational setup and detailed discussion of the flow physics

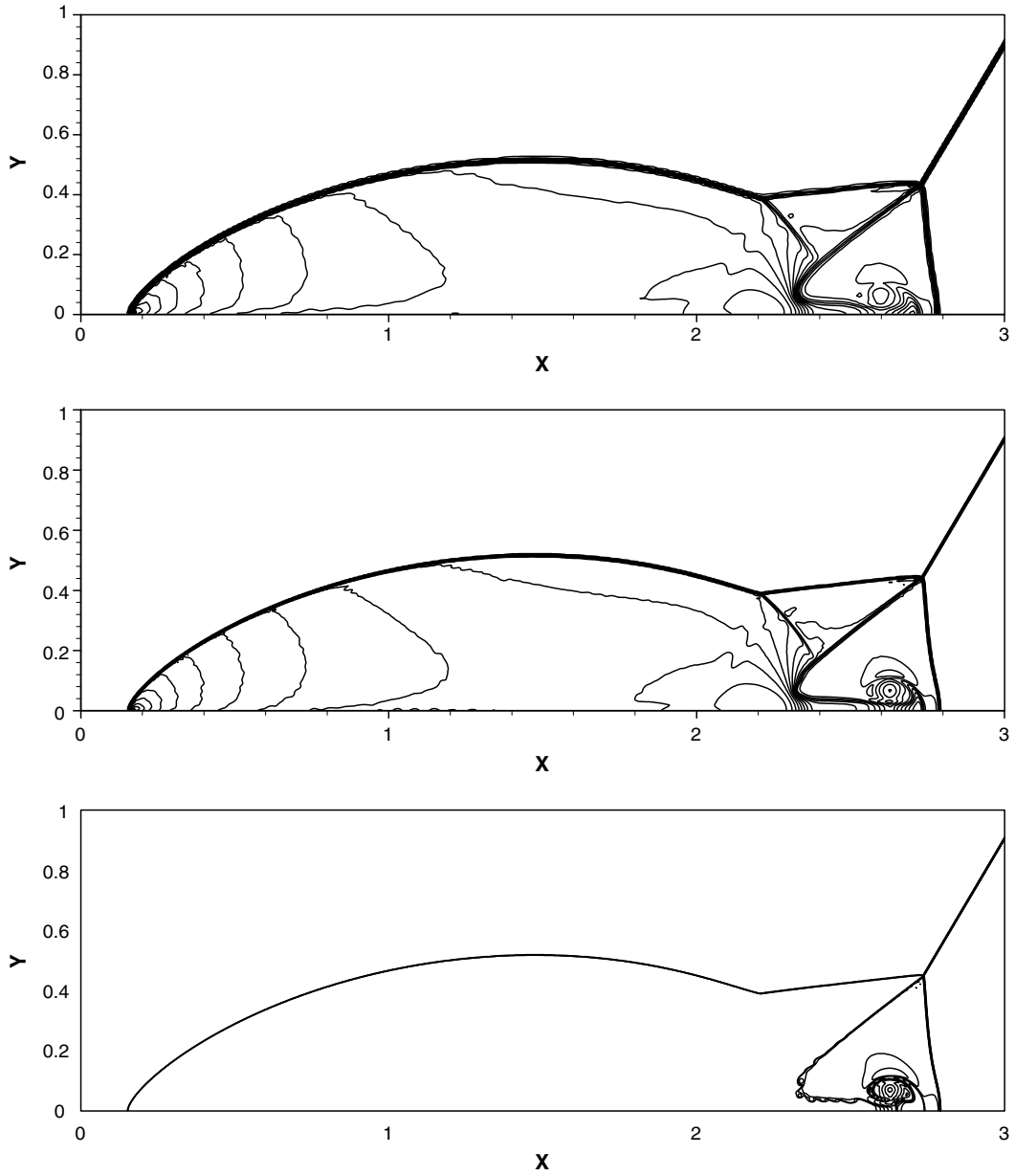

can be found in [47]. At a given output time a complicated flow pattern forms containing two Mach shocks, two slip surfaces and a jet. Figs. 12 and 13 show numerical results from the WENO scheme with the GMUSTA-1 flux of this paper on three meshes: 480×120, 960×240 and 1920×480 cells. We observe that the scheme produces the flow pattern generally accepted in the present literature [47,30] as correct, on all meshes. All discontinuities are well resolved and correctly positioned.

Delicate features of the flow, such as slip surfaces, are generally more difficult to resolve accurately, particularly when using symmetric methods or upwind methods with incomplete Riemann solvers. The results of the present GMUSTA-1 scheme are comparable to those with the *complete* HLLC Riemann solver [45] found in Figs. 2 and 4 of [31], and not reproduced here.

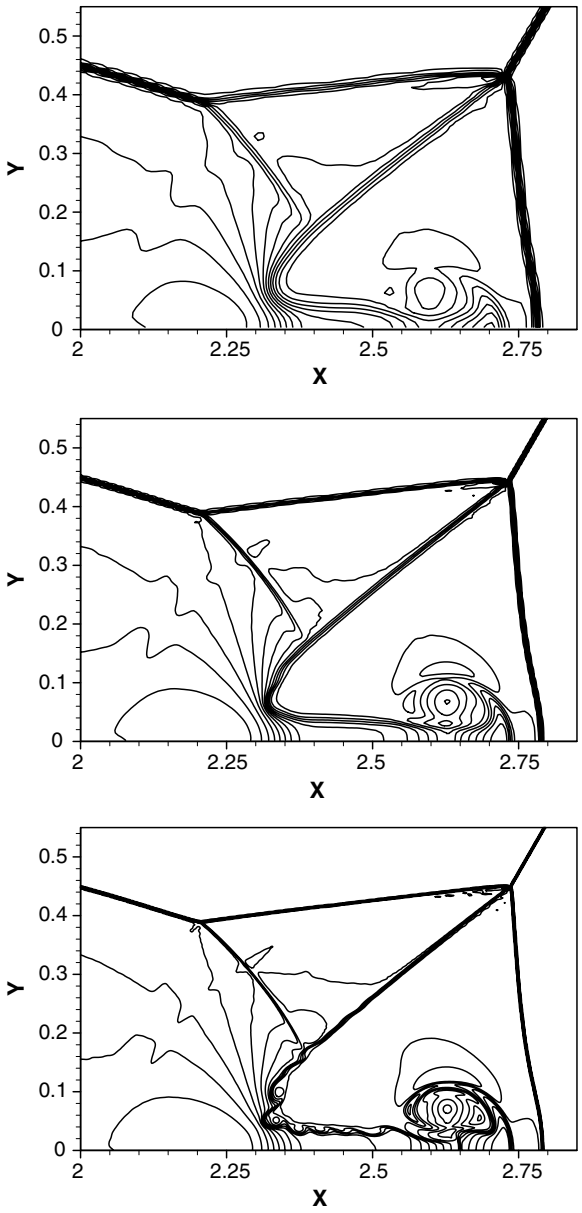

Fig. 13. *Double Mach reflection test problem*. Results from the WENO–GMUSTA-1 scheme. Close-up view of Fig. 12 in the region around the contact surface.

In order to assess the efficiency of the methods presented in this paper in the context of realistic computations we have solved the double Mach reflection problem described above using the WENO method and the high-order ADER method [44,32] on the mesh of 240×60 cells. We tested the GMUSTA fluxes of this paper against a standard complete approximate Riemann solver, the HLLC solver [45,42], which is used to normalize the computing times of other schemes. For the WENO method just described the normalized computing time was 1.0, of course; for the WENO + GMUSTA-1 scheme the figure was 1:125, for WENO + GMUSTA-2 was 1.30 and for WENO + GMUSTA-3 was 1.54. It is worth remarking that for the ADER schemes the CPU times are generally smaller and so are the differences between the MUSTA fluxes and HLLC. Normalizing again by the ADER + HLLC scheme we obtained the figure 1:0 for HLLC, 1.06 for GMUSTA-1, 1.10 for GMUSTA-2 and 1.28 for GMUSTA-3. Numerical experiments show that GMUSTA-1 gives results that are comparable to those of the Godunov method in conjunction with the exact Riemann solver or complete approximate Riemann solvers. Thus we conclude that for the WENO method, GMUSTA-1 is about 12% more expensive than HLLC and for the ADER method, GMUSTA-1 is about 6% more expensive than HLLC. These increases are modest and given the simplicity and generality of the fluxes presented, they are justified.

6. Summary and conclusions

We have first presented a new upwind numerical flux, called GFORCE, that is a generalization of the FORCE symmetric flux. Then we have incorporated this flux into the MUSTA framework, leading to schemes of accuracy that is comparable to that of complete Riemann solvers for non-linear hyperbolic systems. But unlike conventional upwind methods with complete or incomplete Riemann solvers, our schemes are applicable to general systems of hyperbolic conservation laws. For a given vector of conserved variables, a corresponding flux vector and appropriate closure relations, the proposed MUSTA numerical flux is most easily computed. For multi-dimensional problems the unsplit versions of the schemes are linearly stable, unlike those of well-known symmetric fluxes such as Lax-Friedrichs and FORCE. The schemes are directly applicable to problems on general meshes. The fluxes have been used as building blocks for high-order non-linear schemes via the TVD approach and the WENO approach. The performance of the new schemes has been demonstrated via the Euler equation for ideal and covolume gases in one and two space dimensions, and for the equations of Magnetohydrodynamics in one space dimension.

For the test problems considered we have seen that the quality of the results of our methods is comparable to that of the best methods available, namely those for which there are complete non-linear Riemann solvers available. Our methods however are computationally more expensive, of the order of 12% for WENO methods and of the order of 6% for ADER methods. We believe that this modest increase in computational time far outweighs the generality and the ease with which the methods of this paper can be applied to difficult problems, especially to those for which no Riemann solvers are currently available. Our methods are suitable for implementation in an industrial context, where there will necessarily be a continuous revision/upgrading of mathematical models, with the associated tedious (if possible at all) task of rederiving the numerical flux each time the mathematical model is changed.

Acknowledgments

Part of the work was carried out while the first author was an EPSRC senior visiting fellow (Grant GR N09276) at the Isaac Newton Institute for Mathematical Sciences, University of Cambridge, UK, as joint organizer (with P.G. LeFloch and C.M. Dafermos) of the research programme on *Non-linear Hyperbolic Waves in Phase Dynamics and Astrophysics*, Cambridge, January–July 2003. The second author acknowledges the support provided by the Isaac Newton Institute, University of Cambridge, UK, as a participant to the same research programme. The authors thank Professor N.V. Pogorelov for useful discussions on the MHD equations.

Appendix. MUSTA-1 program for the Euler equations

```
*-------------------------------------------------------------------*
*
      SUBROUTINE MUSTA1(QL,QR,P,NC)
C     Purpose: compute the MUSTA-1 flux P() for given data QL,QR,
C              with NC conserved variables
      IMPLICIT  NONE
      INTEGER   NC,J
      REAL      CFLCOE,DTODX,DXODT,QL,QR,FL,FR,P
      DIMENSION QL(3),QR(3),FL(3),FR(3),P(3)
      DATA CFLCOE /0.90/
C     Evaluate fluxes FL, FR on data QL, QR
      CALL FLUVAL(QL,FL)
      CALL FLUVAL(QR,FR)
      CALL MUTIME(QL,QR,CFLCOE,DTODX,DXODT)
C     Compute predictor flux P(), use GFORCE
      CALL GFORCE(QL,QR,FL,FR,P,NC,CFLCOE,DTODX,DXODT)
C     Perform one-stage evolution of data on MUSTA mesh
      DO 10 J = 1,NC
         QL(J) = QL(J) - DTODX*(P(J)  - FL(J))
         QR(J) = QR(J) - DTODX*(FR(J) -  P(J))
 10   CONTINUE
C     Re-compute fluxes FL, FR on evolved data QL, QR
      CALL FLUVAL(QL,FL)
      CALL FLUVAL(QR,FR)
      CALL MUTIME(QL,QR,CFLCOE,DTODX,DXODT)
C     Compute corrector flux P() after 1 stage, use GFORCE
      CALL GFORCE(QL,QR,FL,FR,P,NC,CFLCOE,DTODX,DXODT)
      END
*
*-------------------------------------------------------------------*
*
      SUBROUTINE GFORCE(QL,QR,FL,FR,P,NC,CFLCOE,DTODX,DXODT)
C     Purpose: compute GFORCE flux for conserved variables
C              QL,QR and corresponding fluxes FL,FR

     IMPLICIT NONE
     INTEGER  J,NC
     REAL     CFLCOE,DTODX,DXODT,OMEGA,P,QL,QR,FL,FR,QLW,LXW,LXF
     DIMENSION P(3),QL(3),QR(3),FL(3),FR(3),QLW(3),LXW(3),LXF(3)
```

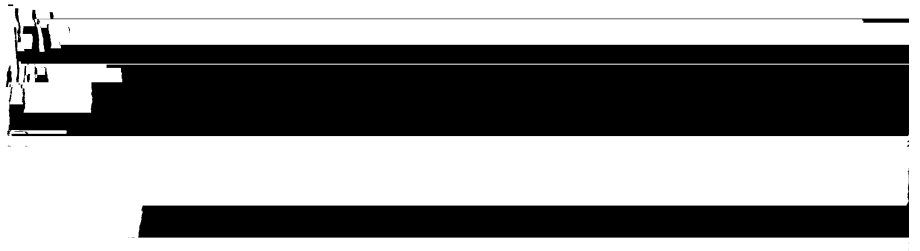

```
*-----------------------------------------------------------------------*
*
      SUBROUTINE MUTIME(QL,QR,CFLCOE,DTODX,DXODT)
C     Purpose: find a time step DT. Mesh spacing is set to DELTA=1
      IMPLICIT NONE
      REAL     GAMMA,CFLCOE,DELTA,DT,DTODX,DXODT,QL,QR,
     &         DL,UL,PL,CL,DR,UR,PR,CR
      DIMENSION QL(3),QR(3)
      COMMON /GAMMAS/ GAMMA
      DELTA = 1.0
      DL    = QL(1)
      UL    = QL(2)/QL(1)
      PL    = (GAMMA-1.0)*(QL(3)-0.5*QL(2)*QL(2)/QL(1))
      CL    = SQRT(GAMMA*PL/DL)
      DR    = QR(1)
      UR    = QR(2)/QR(1)
      PR    = (GAMMA-1.0)*(QR(3)-0.5*QR(2)*QR(2)/QR(1))
      CR    = SQRT(GAMMA*PR/DR)
      DT    = CFLCOE*DELTA/MAX(ABS(UL)+CL,ABS(UR)+CR)
      DTODX = DT/DELTA
      DXODT = DELTA/DT
      END
*
*-----------------------------------------------------------------------*
*
      SUBROUTINE FLUVAL(Q,FLUX)
C     Purpose: evaluate flux vector FLUX() on conserved variables Q()
      IMPLICIT NONE
      REAL     GAMMA,Q,FLUX,P,U
      COMMON /GAMMAS/ GAMMA
      DIMENSION Q(3),FLUX(3)
      U       = Q(2)/Q(1)
      P       = (GAMMA - 1.0)*(Q(3) - 0.5*Q(2)*U)
      FLUX(1) = Q(2)
      FLUX(2) = Q(2)*U + P
      FLUX(3) = (Q(3) + P)*U
      END
*
*-----------------------------------------------------------------------*
*
```

References

[1] A.A. Barmin, A.G. Kulikovskii, N.V. Pogorelov, Shock-capturing approach and nonevolutionary solutions in magnetohydrodynamics, J. Comput. Phys. 126 (1996) 77–90.

[2] S.J. Billett, E.F. Toro, WAF-type schemes for multidimensional hyperbolic conservation laws, J. Comput. Phys. 130 (1997) 1–24.

[3] M. Brio, C.C. Wu, An upwind differencing scheme for the equations of ideal magnetohydrodynamics, J. Comput. Phys. 75 (1988) 400–422.

[4] G.Q. Chen, E.F. Toro, Centred schemes for non-linear hyperbolic equations, J. Hyperbolic Diff. Eq. 1 (1) (2004) 531–566.

[5] P. Colella, Multidimensional upwind methods for hyperbolic conservation laws, J. Comput. Phys. 87 (1990) 171–200.

[6] P. Colella, H.H. Glaz, Efficient solution algorithms for the Riemann problem for real gases, J. Comput. Phys. 59 (1985) 264–289.

[7] R. Courant, E. Isaacson, M. Rees, On the solution of nonlinear hyperbolic differential equations by finite differences, Comm. Pure Appl. Math. 5 (1952) 243–255.

[8] B. Einfeldt, C.D. Munz, P.L. Roe, B. Sjögreen, On Godunov-type methods near low densities, J. Comput. Phys. 92 (1991) 273–295.

[9] P. Glaister, An approximate linearised Riemann solver for the three–dimensional Euler equations for real gases using operator splitting, J. Comput. Phys. 77 (1988) 361–383.

[10] J. Glimm, Solution in the large for nonlinear hyperbolic systems of equations, Comm. Pure Appl. Math. 18 (1965) 697–715.

[11] E. Godlewski, P.A. Raviart, Numerical approximation of hyperbolic systems of conservation laws, Springer, Germany, 1996.

[12] S.K. Godunov, Finite difference methods for the computation of discontinuous solutions of the equations of fluid dynamics, Mater. Sb. 47 (1959) 271–306.
[13] S.K. Godunov, A.V. Zabrodin, G.P. Prokopov, A difference scheme for two-dimensional unsteady aerodynamics, USSR J. Comp. Math. Math. Phys. USSR 2 (6) (1961) 1020–1050.
[14] A. Harten, P.D. Lax, B. van Leer, On upstream differencing and Godunov-type schemes for hyperbolic conservation laws, SIAM Rev. 25 (1) (1983) 35–61.
[15] G.S. Jiang, E. Tadmor, Non-oscillatory central schemes for multi-dimensional hyperbolic conservation laws, SIAM J. Sci. Comput. 19 (6) (1998) 1892–1917.
[16] G.S. Jiang, C.C. Wu, A high-order WENO finite difference scheme for the equations of ideal magnetohydrodynamics, J. Comput. Phys. 150 (1999) 561–594.
[17] A.G. Kulikovskii, N.V. Pogorelov, A.Y. Semenov, Mathematical aspects of numerical solutions of hyperbolic systemsMonographs and Surveys in Pure and Applied Mathematics, Chapman & Hall, London, 2002.
[18] A. Kurganov, E. Tadmor, New high-resolution central schemes for non-linear conservation laws, J. Comput. Phys. 160 (2000) 241–282.
[19] P.D. Lax, B. Wendroff, Systems of conservation laws, Comm. Pure Appl. Math. 13 (1960) 217–237.
[20] R.J. LeVeque, Finite volume methods for hyperbolic problems, Cambridge University Press, Cambridge, 2002.
[21] D. Levy, G. Puppo, G. Russo, A fourth order central WENO scheme for multidimensional hyperbolic systems of conservation laws, SIAM J. Sci. Comput. 24 (2) (2002) 480–506.
[22] R. Liska, B. Wendroff, Composite schemes for conservation laws, SIAM J. Numer. Anal. 35 (6) (1998) 2250–2271.
[23] E.H. Love, F.B. Pidduck, Lagrange's ballistic problem, Phil. Trans. Roy. Soc. Lond. 222 (1922) 167–228.
[24] R. Menikoff, B.J. Plohr, The Riemann problem for fluid flow of real materials, Rev. Modern Phys. 61 (1989) 75–130.
[25] H. Nessyahu, E. Tadmor, Non-oscillatory central differencing for hyperbolic conservation laws, J. Comput. Phys. 87 (1990) 408–463.
[26] V.P. Kolgan, Application of the principle of minimum derivatives to the construction of difference schemes for computing discontinuous solutions of gas dynamics (in Russian), Uch. Zap. TsaGI, Russia 3 (6) (1972) 68–77.
[27] L. Quartapelle, L. Castelletti, A. Guardone, G. Quaranta, Solution of the Riemann problem of classical gas dynamics, J. Comput. Phys. 190 (1) (2003) 118–140.
[28] P.L. Roe, Approximate Riemann solvers, parameter vectors, and difference schemes, J. Comput. Phys. 43 (1981) 357–372.
[29] V.V. Rusanov, Calculation of interaction of non-steady shock waves with obstacles, J. Comput. Math. Phys. USSR 1 (1961) 267–279.
[30] C. Shi, J. Hu, C.W. Shu, A technique for treating negative weights in WENO schemes, J. Comput. Phys. 175 (1) (2002) 108–127.
[31] V.A. Titarev, E.F. Toro, Finite volume WENO schemes for three-dimensional conservation laws, J. Comput. Phys. 201 (1) (2004) 238–260.
[32] V.A. Titarev, E.F. Toro, ADER schemes for three-dimensional hyperbolic systems, J. Comput. Phys. 204 (2005) 715–736.
[33] V.A. Titarev, E.F. Toro, MUSTA schemes for multi-dimensional hyperbolic systems: analysis and improvements, Int. J. Numer. Meth. Fluid 49 (2005) 117–147.
[34] E.F. Toro, Multi-Stage Predictor–Corrector Fluxes for Hyperbolic Equations. Technical Report NI03037-NPA, Isaac Newton Institute for Mathematical Sciences, University of Cambridge, UK, 17th June, 2003.
[35] E.F. Toro, A fast Riemann solver with constant covolume applied to the random choice method, Int. J. Numer. Meth. Fluid 9 (1989) 1145–1164.
[36] E.F. Toro, A weighted average flux method for hyperbolic conservation laws, Proc. Roy. Soc. Lond. A423 (1989) 401–418.
[37] E.F. Toro, Riemann-problem based techniques for computing reactive two-phase flows, in: Dervieux, Larrouturrou (Eds.), Proceedings of the 3rd International Conference on Numerical Combustion, Lecture Notes in Physics, vol. 351, Antibes, France, May, 1989, pp. 472–481.
[38] E.F. Toro, On Glimm-Related Schemes for Conservation Laws. Technical Report MMU-9602, Department of Mathematics and Physics, Manchester Metropolitan University, UK, 1996.
[39] E.F. Toro, Riemann Solvers and Numerical Methods for Fluid Dynamics, second ed., Springer-Verlag, Germany, 1999.
[40] E.F. Toro, Riemann Solvers with Evolved Initial Conditions. Int. J. Numer. Meth. Fluids, 2006 (to appear).
[41] E.F. Toro, S.J. Billett, Centred TVD schemes for hyperbolic conservation laws, IMA J. Numer. Anal. 20 (2000) 47–79.
[42] E.F. Toro, A. Chakraborty, Development of an approximate Riemann solver for the steady supersonic Euler equations, Aeronaut. J. 98 (1994) 325–339.
[43] E.F. Toro, W. Hu, Unsplit centred finite volume schemes: preliminary results, in: E.F. Toro (Ed.), Godunov Methods: Theory and Applications, Kluwer Academic/Plenum Publishers, Dordrecht/New York, 2001.
[44] E.F. Toro, R.C. Millington, L.A.M. Nejad, Towards very high-order Godunov schemes, in: E.F. Toro (Ed.), Godunov Methods: Theory and Applications. Edited Review, Kluwer Academic/Plenum Publishers, Dordrecht/New York, 2001, pp. 905–937.
[45] E.F. Toro, M. Spruce, W. Speares, Restoration of the contact surface in the HLL-Riemann solver, Shock Waves 4 (1994) 25–34.
[46] B. van Leer, Towards the ultimate conservative difference scheme I. The quest for monotonicity, Lect. Notes Phys. 18 (1973) 163–168.
[47] P. Woodward, P. Colella, The numerical simulation of two-dimensional fluid flow with strong shocks, J. Comput. Phys. 54 (1984) 115–173.